Improving the Quality of Low-Cost GPS Receiver Data for Monitoring Using Spatial Correlations

L. Zhang, V. Schwieger
Institute of Engineering Geodesy,
University of Stuttgart, Geschwister-Scholl-Str. 24 D, 70174 Stuttgart, Germany

Abstract. The investigations on low-cost single frequency GPS receivers at the Institute of Engineering Geodesy (IIGS) show that u-blox LEA-6T GPS receivers combined with Trimble Bullet III GPS antennas containing self-constructed L1-optimized choke rings can already obtain an accuracy in the range of millimeters which meets the requirements of geodetic precise monitoring applications (see Zhang and Schwieger 2013). However, the quality (accuracy and reliability) of low-cost GPS receiver data, particularly in shadowing environment, should still be improved, since the multipath effects are the major error for the short baselines.

For this purpose, several adjoined stations with low-cost GPS receivers and antennas were set up next to the metal wall on the roof of the IIGS building and measured statically for several days. The time series of three-dimensional coordinates of the GPS receivers were analyzed. Spatial correlations between the adjoined stations, possibly caused by multipath effect, will be taken into account. The coordinates of one station can be corrected using the spatial correlations of the adjoined stations, so that the quality of the GPS measurements is improved.

The developed algorithms are based on the coordinates and the results will be delivered in near-real-time (in about 30 minutes), so that they are suitable for structural health monitoring applications.

Keywords. Low-cost GPS receiver, multipath effect, spatial correlations analysis, monitoring.

1 Introduction

GNSS receivers are able to measure the 3-dimensional positions automatically and continuously. In order to inform the users of potential dangers as early as possible, GNSS data is evaluated block by block as a near-real-time solution.

The investigations at the Institute of Engineering Geodesy (IIGS) and at other research institutions (Schwieger und Gläser 2005, Schwieger 2007, Schwieger 2008, Schwieger 2009, Limpach 2009, Glabsch et al. 2010) show that accuracies of sub-cm can be achieved even with low-cost single frequency GPS receivers, if the carrier phase measurements of the GNSS receivers are evaluated in relative mode and the length of the baseline is up to several kilometers. Influences of baseline-length-dependent errors, such as ionospheric and tropospheric errors, can be mitigated for short baselines. The monitored objects like landslides or dams have normally an extension up to a couple of kilometers and so the low-cost single-frequency GPS receivers are suitable for these kinds of applications. Apart from that, compared to the geodetic GNSS receivers which may cost more than 20,000 €, the low-cost single frequency GNSS receivers have the advantage to be cost-effective. For example, the u-blox LEA-4T/6T GPS receivers which are investigated at IIGS cost less than 100 €. However, the influence of site-dependent errors particularly the multipath effects cannot be reduced in relative mode, so it is still a general problem for the precise GNSS positioning, particularly in shadowing environment. Multipath effect affects not only the accuracies of relative but also of absolute positioning and it is a limiting factor for accuracies for both geodetic dual-frequency and low-cost single frequency GNSS receivers.

Since the beginning of GPS development, there has been a lot of research on the multipath effect, and different methods have been developed to reduce the multipath effects, such as improving the receiver technology (Van Dierendonck et al. 1992), using the Signal-To-Noise Ratio (Axelrad et al. 1994), applying sidereal filtering (Choi et al. 2004) and station calibration (Wanninger and May 2000), or improving the antenna design (Filippov et al. 1998, Krantz et al. 2001, Kunysz 2003, Tatarnikov et al. 2011). Up to now, there is no method which can completely eliminate the influence of the

multipath effects. And many methods can only be used for post-processed measurements of static objects like reference stations, but they are not suitable for near-real-time kinematic monitoring applications. Besides, many methods are based on the carrier phase measurements which are not accessible to every user of all the GNSS software and hardware. The developed algorithm which will be introduced in this paper is based on the coordinates, and the results will be delivered in near-real-time, so that they are suitable for structural health monitoring applications.

Since the low-cost GPS receivers are cost-effective, many of them can be mounted on monitored objects and high spatial sampling rates can be provided. The multipath effect does not change spatially very quickly, so its influence on adjoined stations should be correlated. The multipath effect can be reduced significantly by using the spatial correlation between several adjoined antennas (Ray et al. 1998). The method in Ray et al. (1998) is carrier phase based. The developed algorithm in this paper is coordinates based.

A test with 9 adjoined antennas is carried out and described in section 2. Their spatial correlations will be analysed in section 3. An algorithm based on spatial correlation will be introduced in section 4. The algorithm is evaluated by static measurement and simulated deformation. The oscillations of the coordinates can be reduced significantly through this method. The accuracy of the measurements can be improved and deformations can be detected more quickly and more reliably.

2 Test Description

In the preliminary research in Zhang und Schwieger (2013) at IIGS, self-constructed L1-optimized choke rings are developed for Trimble Bullet III GPS antennas (cost about 100 €). U-blox LEA-6T GPS receivers combined with this antenna and the L1-optimized choke rings can already reach an accuracy in the range of millimeters which is comparable with geodetic dual-frequency GNSS antennas and receivers. So this low-cost combination is used for the following test.

2.1 Test Scenario

As shown in Fig. 1, a 3×3 antenna array was set up next to the metal wall on the roof of the IIGS-

building, with a distance between two antennas of 0.5 m, so the antenna array has an extension of $1 \text{ m} \times 1 \text{ m}$. Static measurement is carried out for 26 days (from 3 March to 1 April 2014). The GPS raw data are recorded from the 9 receivers at 1 Hz, stored on a PC, evaluated and post-processed. The raw data are in UBX binary format and are converted into RINEX format using the TEQC (TEQC 2014) provided by Unavco (Unavco 2014), and the baseline is processed by software Wa1 provided by Wasoft (Wasoft 2015).

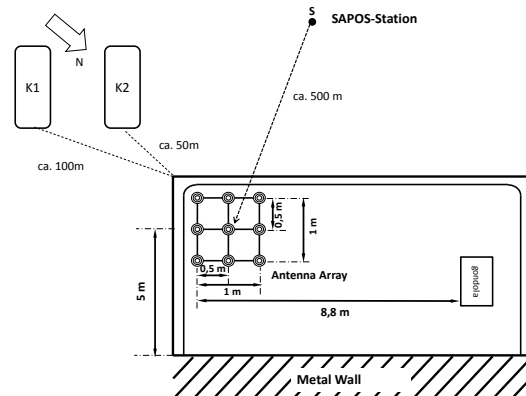**Fig. 1** Photos of test field with antenna array

Fig. 2 Draft of Test Field (not to scale)

SAPOS station (Satellitenpositionierungsdienst der Deutschen Landesvermessung), which is one of the reference stations of the German Satellite Positioning Service, is only about 500 m away from the test field (compare Fig. 2). This station is taken

as reference station and the 9 stations in the test field are taken as rover stations for processing the baselines, so that 9 baselines can be obtained.

2.2 Analysis of the Antenna Surroundings

As it can be seen from Fig. 1, there are many obstructions in the antenna surroundings, but the multipath effect and diffraction are most likely caused by the metal wall (about 4.5 to 5.5 m away), the two high buildings (about 50 m and 100 m away) and the ground (antennas are about 1.2 m above the ground), since the area of the reflector should be bigger than the so-called Fresnel zone to cause multipath effects (Van Nee 1995). The choke rings can reduce the influence of the reflected signal coming from the ground, but they cannot prevent that the antennas from the reflected signal are higher than is the antenna horizon (Weill 1997).

The reflected signal can cause the periodic multipath effect (Georgiadou and Kleusberg 1988) on the carrier phase measurement and the periodic effect can be also found in the coordinates (Heister et al. 1997). In Irsigler (2008), the frequency of multipath on the carrier phase can be estimated for horizontal and vertical reflectors using the equation (1).

$$f_{\delta\varphi}(t) = \frac{2}{\lambda} \cdot \begin{cases} h \cdot \cos E^s(t) \cdot \dot{E}^s(t) & \text{horizontal} \\ -d \cdot \sin E^s(t) \cdot \dot{E}^s(t) & \text{vertical} \end{cases} \quad (1)$$

λ is the wavelength, it is 19 cm approximately for the L1 frequency. h and d are the vertical and horizontal distances between the antenna and the reflector. The closer the reflector is located, the longer is the period. E^s and $\dot{E}^s$ are the elevation of the satellite and its change over time (velocity). A satellite with high elevation can cause long and short periodic multipath effects respectively for horizontal and vertical reflectors. The faster the satellite is moving, the shorter is the period of the multipath effect. The wavelength is constant, for one antenna the distance h and d does not change so much even for monitoring application. However, the elevation of the satellite changes all the time and the velocity of elevation is not constant, either. For this reason, the frequency of multipath effects varies all the time. Using the mean value of the velocity of the elevation 0.07 mrad/s and equation (1), the period caused by multipath effects can be calculated. The one caused by the ground should be more than 20 minutes, and that from the metal wall

varies from several minutes to half an hour. The two high buildings can cause multipath effects with periods of up to two minutes. Normally the antennas are affected by the multipath effects from several reflectors and several satellites. Therefore, in practice the multipath effect is a combination of many harmonic oscillations, and its mean value is not zero particularly within short time.

Besides, equation (1) shows that the multipath effect is spatially correlated, the adjoined antennas have different distances to the reflector, but the velocity of elevation is the same for every antenna; the elevations are slightly different, so that a similar multipath can be found at adjoined antennas.

3 Analysis of Temporal and Spatial Correlations

The results of Wa1 are the baseline in the UTM-system in east, north and height for every second. The outliers in the coordinate's time series, which are probably caused by the unfixed ambiguities, are detected according to the 3σ-rule and linear interpolated, and the standard deviation is calculated. The percentage of outliers and the standard deviation are regarded as parameter for describing the reliability and accuracy of the measurements, respectively, and reliability and accuracy is two parameters to describe to quality of GPS measurement (Zhang 2015).
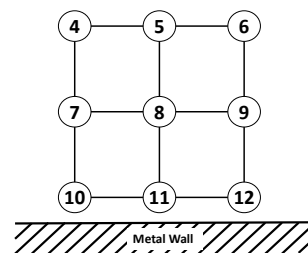

Fig. 3 Antenna number

The 9 antennas are numbered (compare Fig. 3). Fig. 4 to Fig. 7 show exemplarily the standard deviations and percentages of outliers of the 26 daily solutions of baselines s-a4 and s-a10.

The results of baseline s-a4 are more accurate and reliable than that of baseline s-a10 (compare Fig. 4 with Fig. 5 and Fig. 6 with Fig. 7), since antenna a10 is closer to the wall than antenna a4. The baseline s-a4 has a standard deviation σ_E=3.2 mm, σ_N=5.6 mm and σ_h=9.0 mm. The baseline s-a10 has

a standard deviation σ_E=3.7 mm, σ_N=6.1 mm and σ_h=9.7 mm. About 2% and 3% of the data are detected as outliers in the time series of baseline s-a4 and s-a10 respectively. The variations of the daily solutions of the baseline s-a4 and s-a10 is similar, since both antennas are influenced by the multipath from the wall, the similarity of coordinate series between the baselines will be discussed later.
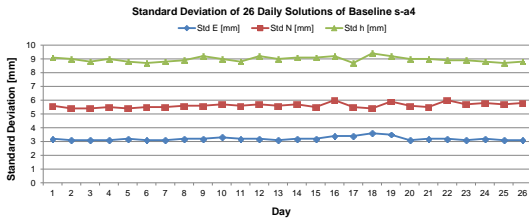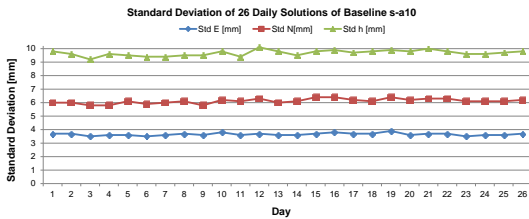

Fig. 4 Standard Deviations of the 26 daily solutions of baseline s-a4

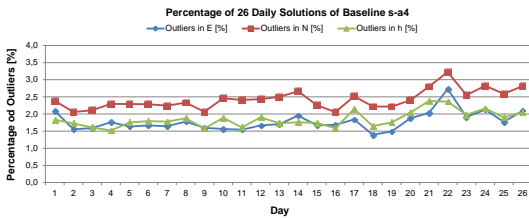**Fig. 5** Standard Deviations of the 26 daily solutions of baseline s-a10

Fig. 6 Rate of Outliers of the 26 daily solutions of baseline s-a4
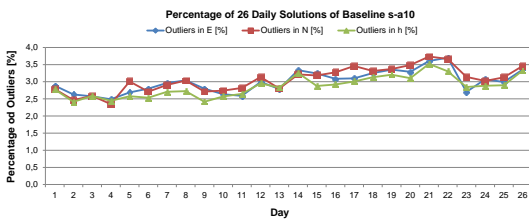

Fig. 7 Rate of Outliers of the 26 daily solutions of baseline s-a10

The daily solutions vary a little day by day because of the slight change of satellite orbits, however they are still quite similar. For this reason, the data of the last day is chosen for the following analysis in this paper.

The standard deviations in the position and mean percentage of outliers (the mean of all the coordinate components) of all the 9 baselines (of the last day) are shown in Fig. 8 and Fig. 9.
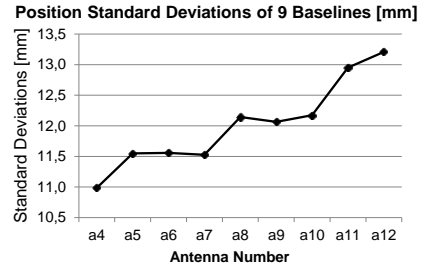

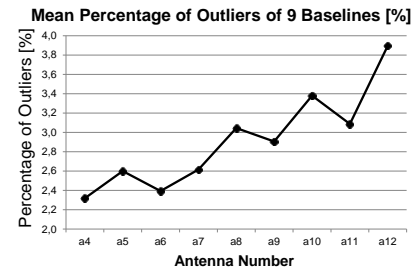**Fig. 8** Position Standard deviations of 9 Baselines

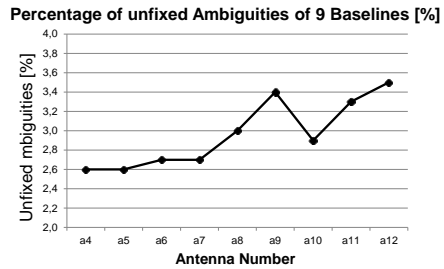**Fig. 9** Mean Percentage of Outliers of 9 Baselines

Fig. 10 Percentage of unfixed Ambiguities of 9 Baselines

Generally, the closer the antenna is to the wall, the stronger is influence of the multipath effect on the antennas and the worse is the quality of the measurements, since the ambiguities will be more difficult to be fixed (compare Fig. 10). For example, the baseline s-a4 has a 2.3 % of outliers and a standard deviation (position) of 11.0 mm, while the s-a12 has a 3.9 % of outliers and a standard deviation (position) of 13.2 mm. The percentage of the outliers and the unfixed ambiguities fit quite well. However they are not the same, probably because some ambiguities are fixed but to wrong integers. The accuracy and reliability as well as the percentage of the unfixed ambiguities of the baselines varies also within the same row, it is

4

probably because of the gondola (about 8.8 m on the right side of the antenna array, compare Fig. 2)

The autocorrelation function (compare equation (2)) can be used to analyze the temporal correlations of the time series:

$$\hat{R}_{XX}(m) = \frac{\sum_{i=1}^{n-m}(x_i-\bar{x})(x_{i+m}-\bar{x})}{s_X^2 \cdot (n-m-1)}. \qquad (2)$$

x is the time series, $\bar{x}$ and s_X are the mean value and standard deviation of x. n is the length of the time series and the autocorrelation functions can be calculated reliably until $m = n/10$ (Chatfield 1989).

Generally, the errors of the GPS measurement can be classified to correlating and non-correlating errors (Schwieger 1999). Fig. 11 shows the autocorrelation function of baseline s-a4 as an example. It is evident, that autocorrelation functions decline quickly between of 0 to 1 second, and then they fall exponentially with oscillations. This effect indicates that the three coordinate components are combinations of the white, red and colored noise processes. The white noise is neither temporally nor spatially correlated and can be regarded as non-correlating error. The white noise of the coordinates comes mainly from the GPS receiver. The red and colored noise can be regarded as correlating errors; the colored noise shows that the coordinate contains periodic oscillations which match the property of multipath effects.
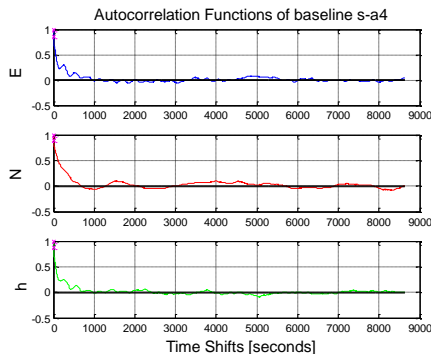

Fig. 11 Autocorrelation functions of baseline s-a4

Moreover, in Fig. 11 only the autocorrelation of the daily solution is shown to give an overview of the property of the process. If e.g. the autocorrelation functions are calculated for every hour, it can be seen that the autocorrelation functions and also mean values vary from time to time, that is probably because of the multipath effect. This phenomenon indicates that GPS coordinates time series are non-stationary processes (Chatfield 1989).

While the autocorrelation function describes the temporal correlation of one-time series with itself, the cross-correlation function

$$\hat{R}_{XY}(m) = \frac{\sum_{i=1}^{n-m}(x_i-\bar{x})(y_{i+m}-\bar{y})}{s_X \cdot s_Y \cdot (n-m-1)}, \qquad (3)$$

can be used to describe the correlation between two-time series x and y.

For example, the cross-correlation functions between the baseline s-a4 and s-a5 can be calculated, as shown in Fig. 12, and the spatial correlation between these two baselines can be described. Fig. 12 shows that the cross-correlation functions are not symmetrical and the maximum of the cross-correlation function is not 1, since some error, e.g. the white noise of station a4 and a5, are different and they are not correlated. Besides, the phenomenon that the residues of coordinates are a combination of correlating and non-correlating errors can be seen from Fig. 12.
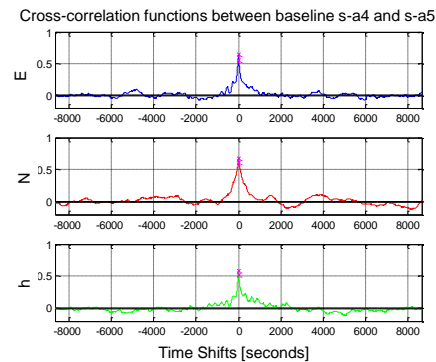

Fig. 12 Cross-correlation functions between baseline s-a4 and s-a5

The cross-correlation functions can be calculated for different combinations of baselines, their maximums are different. In Fig. 13, the maximum of the cross-correlation functions between baseline s-a4 and the other baselines is shown. Since antenna 8 stands in the middle of the array, the maximum spatial correlation between baseline s-a8 and other baselines is shown in Fig. 14.

From both figures it can be seen that the correlations of the errors are not only dependent on distance between the antennas, but also on the direction. It means that the errors do not change spatially linear.
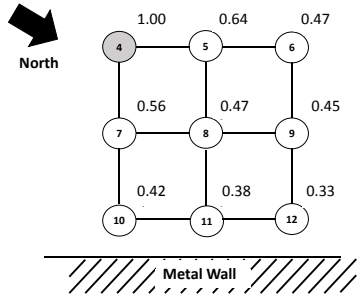
Fig. 13 Maximum spatial correlation between baseline s-a4 and the other baselines respectively
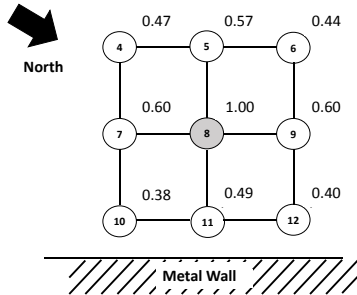

Fig. 14 Maximum spatial correlation between baseline s-8 and the other baselines respectively

Furthermore, both the autocorrelation functions and cross-correlation functions drop down to zero after about 1000 seconds (or about 15 minutes), although some long-term periods can be recognized. This means that the short-term temporal and spatial correlation of the coordinate components can be ignored with a time shift of about 1000 seconds. For this reason, the coordinates will be evaluated in a 15-minutes block and simulate the near-real time processing. The GPS receivers need some time to get fixed solusion. In test field in Zhang and Schwieger (2013), the U-blox LEA-6T GPS receivers can get fixed solution in 10 minutes, if the antennas have open sky. If there are some obstructions, it needs about 15 to 20 minutes to get the fixed solution. In the test field in this paper there are many obstructions (compare Fig. 1 and Fig. 2), to get a reliable coordinates time series, one daily solution is used and it is divided into 96 15-minutes blocks.

4 Improvement using Spatial Correlations

The coordinate residuals contain both non-correlating and correlating errors. Only the correlated errors are of interest. The non-correlating errors are reduced by using the moving average filter. By analysing the coordinates, it is noticed that the coordinates often contain oscillations with periods of 30 to 40 seconds. These periods are probably caused by the multipath effects from the two high buildings (Zhang 2015). These periods are so short that they are not really of interest for monitoring. For this reason, 40 seconds are chosen as window size of the moving average.

In Fig. 15 and Fig. 16 , the smoothed baselines s-a4 and s-a5, and their cross-correlation functions of the first 15-minutes block are shown.

It can be found out that their residuals can be quite similar (compare east and height component) and sometimes not (compare north component), and there are time shifts between their errors. That means that similar errors can be present in baseline s-a4 as well as in baseline s-a5 with a time shift.
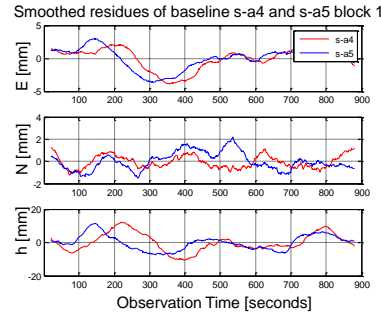

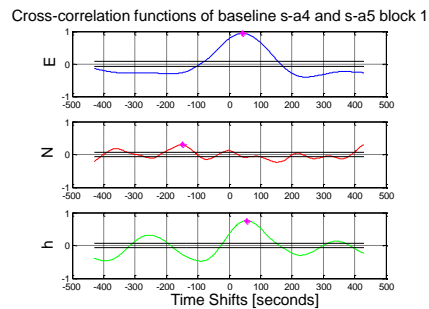**Fig. 15** Smoothed baselines s-a4 and s-a5

Fig. 16 Cross-correlation functions between smoothed baselines s-a4 and s-a5

The absolute values of the time shift here in block 1 is 44, 147 and 59 seconds for the east, north and height components. The block 1 is just an example, the time shifts vary from block to block and they can be positive or negative as well as zero. Also the correlations of each coordinates component vary from block to block. They depend on geometry of satellite-antenna-reflector.

6

So, the idea of the algorithm is that the coordinates of one station (station A) can be corrected using the spatial correlations of coordinates of an adjoined station (station B), so that the accuracy and reliability of the GPS measurement is improved:

$$kr_{\overline{SA},j,q}(t) = k_{\overline{SA},j,q}(t) - m_{j,q} \cdot k_{\overline{SB},j,q}(t + \Delta t). \qquad (4)$$

As shown in equation (4), $k_{\overline{SA},j,q}(t)$ and $k_{\overline{SB},j,q}(t)$ are residuals of two baselines in j-component (j=1,2,3) and q block (q=1,2, …96). These residuals are free from the mean value. The geometry relationship between the station S, A, B is used to correct part of the errors from the GPS-processing, it will not be explained here, the details can be found in Zhang (2015). It can be derived from the cross-correlation function that two residuals $k_{\overline{SA},j,q}(t)$ and $k_{\overline{SB},j,q}(t)$ have the maximum of correlation at time shift Δt. $k_{\overline{SB},j,q}(t)$ will be taken and shifted about Δt, so that we can achieve $k_{\overline{SB},j,q}(t + \Delta t)$. It is assumed that there is scale $m_{j,q}$ between $k_{\overline{SA},j,q}(t)$ and $k_{\overline{SB},j,q}(t + \Delta t)$, so $k_{\overline{SB},j,q}(t + \Delta t)$ will be scaled and used to correct the $k_{\overline{SA},j,q}(t)$, the corrected residuals for the baseline SA is $kr_{\overline{SA},j,q}(t)$. The maximum of the cross-correlation function can be taken as scale $m_{j,q}$, or $m_{j,q}$ can be estimated by adjustment. The scale calculated by adjustment can provide better results (Zhang 2015), since the scale larger than 1 (compare equation (4)) is a possible solution for some cases, this cannot be delivered by correlation functions.

For example a4 and a5 are regarded as station A and B. The residuals of baseline s-a5 can be taken to correct the residuals of baseline s-a4. In Fig. 17 the residuals of baseline s-a5 are shifted about Δt and compared with the baseline s-a4.
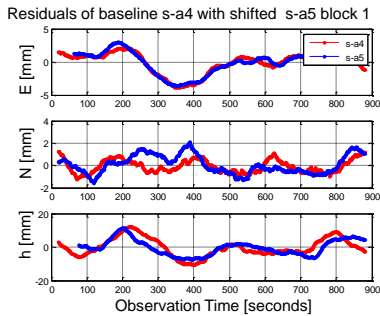

Fig. 17 Residuals of baseline s-a4 with shifted s-a5

The residuals of baseline s-a4 $k_{\overline{sa4},j,q}(t)$ and the corrected s-a4 $kr_{\overline{sa4},j,q}(t)$ using $k_{\overline{sa5},j,q}(t)$ according the equation (4) are shown in Fig. 18. The performance of this algorithm is dependent on the spatial correlation. In Fig. 18 it can be seen that oscillations in the east and height component are significantly suppressed, since the correlations between these two components are very high. The correction does not work well in the north component, since the correlation is quite low.
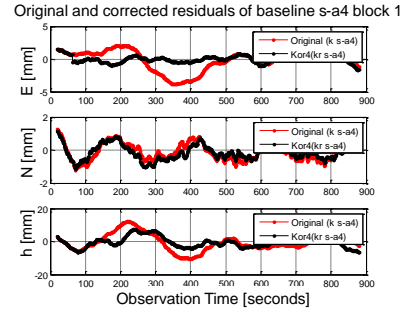

Fig. 18 Original and the corrected s-a4

The spatial correlation varies from time to time. Thus, the performance of the algorithm will be evaluated in section 5 for all 96 blocks and the results will be shown and discussed.

5 Evaluation by Simulated Deformation

The residuals of all 9 baselines are divided into blocks of 15 minutes. Antenna a4 is taken as station A and all other antennas are regarded as station B to correct the residuals of baseline s-a4. For static measurements, compared to the standard deviation of original residuals, the standard deviation of baseline s-a4 (position) is improved by 19 % through smoothing and by about 37 % to 52 % through applying the spatial based algorithm which is described in section 4. The degree of improvement depends on which baseline is used for the correction. Generally, the higher the spatial correlation, the more the standard deviation of baseline s-a4 can be improved. The details about the evaluation of the static measurements will not be described in this paper, since the focus is on the measurements including simulated deformations.

Step and linear deformations are typical deformations for landslides. The real landslide deformation is normally a combination of both. The

7

linear deformation can be regarded as a special case of the step deformation, so the algorithm is evaluated with step deformation. Step deformations are simulated to the amount of the respective standard deviation. For the baseline s-a4 σ_E=3.2 mm, σ_N=5.6 mm and σ_h=9.0 mm (from daily solution) are taken as values for the step deformation for each coordinate component. The step deformation is simulated in the middle of the first block (at 450th second). It is assumed that the same deformations occur at the same time for all stations.

In Fig. 19 the smoothed residuals with the deformation of baseline s-a4 and s-a5 and their cross-correlation functions are shown in Fig. 20.

These simulated step deformations are added to the static measurements of the first block. The effect on the coordinates is that the first block has a positive offset of 0.5 σ, and the other blocks have a positive offset of 1σ in every coordinate component. That means that all the 96 blocks have deformations.
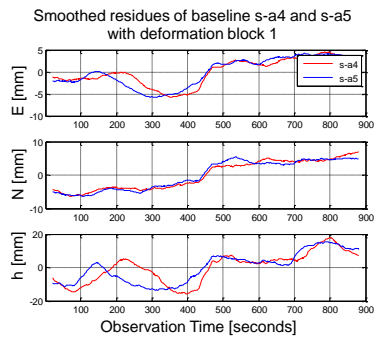

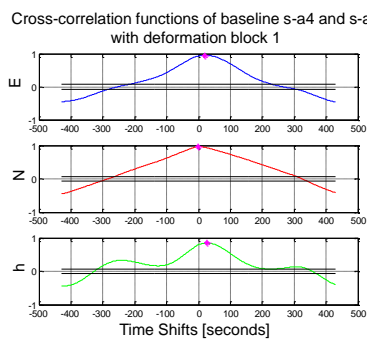**Fig. 19** Smoothed baselines with deformation

Fig. 20 Cross-correlation functions between smoothed baseline s-a4 and s-a5 with deformation

If Fig. 19 and Fig. 20 are compared with Fig. 15 and Fig. 16, it can be recognized that due to the

same deformation at the same time, the maximum of the correlation increases and the time shift for the maximum approaches zero seconds.

It should be noticed that, as described in section 3, the coordinates are not stationary. The original residuals of the daily solution are reduced by the mean value of the whole day and not by that of the block. So even if there are no deformations, the mean values of residuals of blocks are not zero, the standard deviation differs from block to block.

For the deformation analysis, the standard deviation and mean value for each block can be calculated, and the mean value may be tested for the significance by equation (5):

$$T_{j,q} = \left| \frac{\bar{x}_{j,q}}{s_{j,q}} \right| \sim t_{f,95\%}. \qquad (5)$$

If the test value $T_{j,q}$ exceeds for example the quantile $t_{f,95\%}$ (t-distribution) a deformation is detected (with a probability of 95 %). Since the number of observations is large, the Gaussian distribution can be used as approximation for t-distribution. The developed algorithm can decrease the standard deviations, so that the probability to detect the deformation is increased.

Before applying the developed algorithm, the mean value will be subtracted from the residuals of the block. This mean value contains part of the error budget as well as the potential deformation. For this reason, this mean value will be added again to the residuals, after applying the algorithm. The effect is that the mean value is almost unchanged through the algorithm, but the standard deviation of the residue is smaller, because the oscillations in the coordinates are reduced. As a result, the test value T is larger and the probability that deformations can be detected will be higher and earlier.

If the algorithm is not applied, the detection quota of deformations with 1σ is 18.8 %, 24.0 % and 16.7 % for east, north and height components, so it is 19.8 % on average. By using this algorithm and taking the baseline s-a5 for correction, the detection quota of deformation turns out to be 74.0 %, 78.1 % and 65.6 % for each component, and 72.6 % on average. So the improvement is about 50%.

Fig. 21 shows the detection quota on average if all other baselines are taken as correction for baseline s-a4. The result also matches the spatial correlation (compare Fig. 13) quite well, the higher the spatial correlation is, and the better is the performance of the developed algorithm.
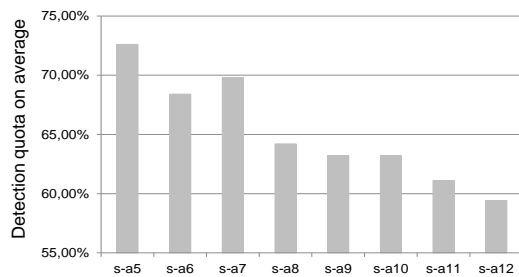
Fig. 21 Detection quota of deformation of baseline s-a4 using all other baselines

Furthermore, it should be noticed that the sensitivity for detection of the deformation is increased through the developed algorithm. The probability of a false alarm is also higher. That is because this algorithm can only reduce oscillations with short periods. Some multipath effects cause oscillations with long periods. These cannot be separated from real deformations. The mean value that is taken from the coordinate contains part of the multipath error and also of the deformation. To avoid false alarms, one may accept a deformation only in case of detection in two neighboring blocks. Real step or linear deformations will be kept in the coordinates. In contrast, the long periodic oscillation coordinates behavior is elastic. It should also be noticed that this algorithm can be applied for the detection of the step and linear deformation, but not for the periodic deformation. So, in this way, the step and linear deformation can be detected more quickly and more reliably in near real-time with a time delay of 30 minutes, more details can be found in Zhang (2015).

In the future, the problem that part of the error cannot be separated from the real deformation should be solved, probably in combination with other algorithms.

6 Conclusion

In this paper, the spatial correlation of coordinates measured by a low-cost GPS antenna array is analyzed. An algorithm based on spatial correlation of the coordinates is developed. Part of the errors, particularly the oscillating errors of one station (or baseline), can be corrected by an adjoined station (or baseline). The standard deviation of the measurement can be significantly improved by about 50%. Generally, the higher the spatial correlation is, the better works the algorithm. In case of monitoring applications with step and linear

deformation, the algorithm can help to detect the deformation more quickly and reliably. The improvement of probability for detection of deformation of 1σ is about 50%, and a reliable detection in 30 minutes is possible.

Thus this paper shows the possibility of the low-cost GPS antenna array or in any case two antennas with the spatial correlation-based algorithm for the structural health monitoring applications, particularly in the case that the multipath effect are high. In the future the algorithm should be evaluated and improved for real monitoring objects like landside, and the method should be adapted if it is applied for monitoring the buildings and bridges which have periodic deformations.

References

Axelrad, P.; Comp, C.; MacDoran, P. (1994): Use of Signal-To-Noise Ratio for Multipath Error Correction in GPS Differential Phase Measurements: Methodology and Experimental Results. In: *Proceedings of the 7th International Technical Meeting of the Satellite Division of the Institute of Navigation,* Salt Lake City, pp. 655-666.

Chatfield, C. (1989): The Analysis of Time Series: An Introduction. 4th Edition, Chapman and Hall, New York.

Choi, K.; Bilich, A.; Larson, K. M.; Axelrad, P. (2004): Modified sidereal filtering: Implications for high-rate GPS positioning. Geophysical Research Letters, doi: 10.1029/2004GL021621.

Filippov, V.; Tatarnicov, D.; Ashjaee, J.; Astakhov, A.; Sutiagin, I. (1998): The First Dual-Depth Dual-Frequency Choke Ring. In: *Proceedings of the 11th International Technical Meeting of the Satellite Division of The Institute of Navigation,* Nashville.

Georgiadou, Y; Kleusberg, A. (1988): On Carrier Signal Multipath Effects in relative GPS Positioning. Manuscripta Geodaetica, Band 13, pp. 172-199.

Glabsch, J.; Heunecke, O.; Pink, S.; Schubäck, S. (2010): Nutzung von Low-Cost GNSS Empfängern für ingenieurgeodätische Überwachungsaufgaben. In: *GNSS 2010 - Vermessung und Navigation im 21. Jahrhundert.* DVW-Schriftenreihe, Band 63, Wißner-Verlag, Augsburg, pp. 113-129.

Heister, H.; Hollmann, R.; Lang, M. (1997): Multipath-Einfluß bei GPS-Phasenmessungen: Auswirkungen und Konsequenzen für praktische Messungen. In: *AVN, Band 5*, pp. 166-177.

Irsigler, M. (2008): Multipath Propagation, Mitigation and Monitoring in the Light of Galileo and the Modernized GPS. Dissertation, Bundeswehr University Munich.

Ray, J. K.; Cannon, M. E.; Fenton, P. (1998): Mitigation of Static Carrier Phase Multipath Effects Using Multiple Closely-Spaced Antennas. In: *Proceedings of the 11th International Technical Meeting of the Satellite Division of the Institute of Navigation, Nashville*, pp. 1025-1034.

Krantz, E.; Riley, S.; Large, P. (2001): The Design and Performance of the Zephyr Geodetic Antenna. In:

Proceedings of the 14th International Technical Meeting of the Satellite Division of The Institute of Navigation, Salt Lake City, pp. 11-14.

Kunysz, W. (2003): A Three Dimensional Choke Ring Ground Plane Antenna. In: *Proceedings of the 16th International Technical Meeting of the Satellite Division of the Institute of Navigation,* Portland, pp. 1883-1888.

Limpach, P. (2009): Rock glacier monitoring with low-cost GPS: Case study at Dirru glacier, Mattertal. AHORN, Zurich.

Tatarnikov, D.; Astakhov, A.; Stepanenko, A. (2011): Convex GNSS Reference Station Antenna. In: Proceeding of *International Conference on Multimedia Technology (ICMT),* Hangzhou, pp. 6288-6291.

TEQC (2014): http://facility.unavco.org/software/teqc /teqc.html. Last Access: 30.02.2014.

Unavco (2014): https://www.unavco.org. Last Access: 23.11.2014.

Van Dierendonck, A. J.; Fenton, P.; Ford, T. (1992): Theory and Performance of Narrow Correlator Spacing in a GPS Receiver. In: *Navigation: Journal of the Institute of Navigation, Volume 39, Issue 3*, pp. 265-283.

Van Nee, R. D. J. (1995): Multipath and multi-transmitter interference in spread-spectrum communication and navigation systems. Dissertation, Technische Universität Delft.

Wasoft (2015): http://www.wasoft.de/. Last Access: 23.09.2015.

Wanninger, L.; May, M. (2000): Carrier Phase Multipath Calibration of GPS Reference Stations. In: *Proceedings of ION GPS 2000, Salt Lake City*, pp. 132-144.

Weill, L. R. (1997): Conquering Multipath: The GPS Accuracy Battle. In: *GPS World, Volume 8, Issue 4*, pp. 59-66.

Schwieger, V. (1999): Ein Elementarfehlermodell für GPS-Überwachungsmessungen - Konstruktion und Bedeutung interepochaler Korrelationen. Dissertation, Universität Hannover, Mitteilungen 231.

Schwieger, V.; Gläser, A. (2005): Possibilities of Low Cost GPS Technology for Precise Geodetic Applications. In: *Proceedings on FIG Working Week,* Kairo.

Schwieger, V. (2007): High-Sensitivity GNSS - the Low-Cost Future of GPS?. In: *Proceedings on FIG Working Week*, Hongkong.

Schwieger, V. (2008): High-Sensitivity GPS - an availability, reliability and accuracy test. In: *Proceedings on FIG Working Week,* Stockholm.

Schwieger, V. (2009): Accurate High-Sensitivity GPS for Short Baselines. In: *Proceedings on FIG Working Week,* Eilat.

Zhang, L.; Schwieger, V. (2013): Monitoring mit Low-Cost GPS Empfängern - Chancen und Grenzen. In: *124. DVW-Seminar,* Wißner Verlag, Augsburg.

Zhang, L. (2015): Qualitätssteigerung von Low-Cost-GPS Zeitreihen für Monitoring Applikationen durch zeitlich-räumliche Korrelationsanalyse, Dissertation in printing, University of Stuttgart.